Progress In Electromagnetics Research C, Vol. 137, 185–198, 2023

Compact Dual-Polarized Reconfigurable MIMO Antenna Based on a Varactor Diode for 5G Mobile Terminal Applications

Qasim H. Kareem[1, *], Rana A. Shihab[2], and Hussien H. Kareem[3]

Abstract—With the rapid growth of wireless communication systems, there is a rising demand for multi-input multi-output (MIMO) antenna systems capable of adapting to various frequency bands and operating conditions. This paper presents an integrated design for MIMO antennas based on a varactor diode as a promising component for achieving frequency agility in the proposed system. A dual-polarized system is achieved by employing a combination of two antennas. One antenna is situated on the exterior surface of the side-edge frame, while the other is positioned on the substrate surface. The spatial configuration enables the creation of orthogonal polarization orientations, specifically vertical and horizontal polarizations. In each element, varactor diodes are positioned to provide reactive loading. By incorporating varactor diodes with a variable bias voltage (0.5–10 V) into the antenna design, the resonant frequency can be dynamically adjusted, allowing the antenna to operate across a wide range of frequencies (4.3 to 6.5 GHz) with more than 18 dB of mutual coupling in the working band. The presented reconfigurable antennas are printed on compact dimensions of $15 \times 25 \times 0.8\,\text{mm}^3$ using a Rogers RT5880 material with a relative dielectric constant 2.2. Because of its flexible frequency range, extensive tuning range, small size, and planar structure, it is well-suited for various current and future wireless communication applications, including cognitive radio, software-defined radio, and next-generation wireless networks.

1. INTRODUCTION

Due to the rapid development of wireless communication systems, there is an increasing demand for portable handheld devices with exceptional data rates. While 4G technology is being extensively researched to improve data rates for Long Term Evolution (LTE), the upcoming 5G communication technology is now receiving more attention and interest [1]. The 5G spectrum comprises dual-bands: a millimeter wave and a sub-6 GHz band. The primary obstacle for smartphone is finding a way to incorporate high-performance 5G antennas without interfering with the existing 4G antennas [2]. Because there is currently no universal standard for 5G communication, massive MIMO systems have emerged as a core technology for 5G [3]. However, integrating a massive MIMO antenna on a smartphones can lead to reduced isolation and efficiency due to the large number of antennas that need to be placed in the limited space [provided by the smartphone]. This challenge has made it difficult for antenna designers to deploy multiple antennas on a 5G smartphone while minimizing system integration problems in small areas.

Incorporating antenna reconfigurability, miniaturization, and decoupling techniques is essential to achieving a densely packed configuration of radiators and optimal isolation. This is a compelling topic for antenna engineers attempting to design future antennas. Furthermore, constructing a suitable MIMO antenna array for smartphones requires consideration of additional requirements, such as low-profile design, simplicity of manufacture, and high isolation [4–8]. In recent years, numerous 5G MIMO antenna proposals for mobile terminals operating in the sub-6 GHz band have been published [9–13].

Received 22 July 2023, Accepted 22 August 2023, Scheduled 9 September 2023

* Corresponding author: Qasim Hadi Kareem (qasim.hadi2017@gmail.com).

[1] Electrical Engineering Department, Al-Iraqia University, Iraq. [2] QA & Accreditation Department, University of Baghdad, Iraq. [3] Optics Techniques Department, Dijlah University College, Iraq.

Numerous antenna configurations have been proposed for frequency reconfigurable systems, including monopole, loop, and Printed-IFA. Despite this, an antenna with a single slit in the ground plane has garnered interest due to its small size and potential for seamless integration with various components. This work aims to design, simulate, and fabricate reconfigurable antennas while investigating the viability of incorporating varactor diodes as integrated tuning components to control frequency and radiation patterns. Recent academic articles describe several antennas that can change frequency [9–16]. These antennas work in the frequency range of 1.5–4.35 GHz and use varactor diodes, pin diodes, or micro-electromechanical system (MEMS) switches to change their frequency.

A patch antenna with a slot configuration that can be switched between 1.98 and 3.59 GHz using five radio frequency (RF) PIN diode switches is presented in [9]. The frequency reconfigurability of this design is one of its advantages, as it enables operation in multiple frequency bands. Due to multiple switches, the network may need more bandwidth and complexity. Ref. [10] describes a slot-patch frequency-reconfigurable antenna with a reflector. This antenna can reconfigure its operating frequency between 1.7 and 3.5 GHz. The patch antenna generates three directional frequency bands, and the slot antenna generates three bidirectional frequency bands, among the benefits. However, having both patch and slot antennas may increase the overall size and complexity of the design. Ref. [11] proposes a PIN-diode-based frequency-reconfigurable circular patch antenna. This circular patch antenna has an arc-shaped ground layer slot. Three PIN diodes in the arc-shaped slot reconfigure frequency. Full-wave simulation and experimental testing characterize antenna radiation performance. By regulating PIN switches, six frequency bands can be swapped with similar radiation patterns. [12] presents four PIN diodes on each corner of a rectangular patch antenna to create a frequency-reconfigurable antenna. Three PIN-diode switching designs change the current route and operating frequency. Two approaches — ideal with a metal component and schematic with a PIN diode equivalent circuit — provide simulated outcomes.

In [13], the authors propose a WIMAX and X-band reconfigurable antenna with circular slots. Coplanar waveguide (CPW) feeding based-PIN diodes are used for tuning frequency reconfigurable antennas. Dual-band operation is made possible by a T-shaped resonator placed in the circular slot and a parallel resonator in the transmission line. Using PIN diodes in the circular slot to swap frequencies, the design can be switched between the WiMAX band (3–4.1 GHz) and the X-band (10.7–11.3 GHz). In [14], a dual-band reconfigurable patch antenna with pattern control is presented. Eight rectangular openings enable low-band directional radiation pattern adjustment via current distribution control. Even though the design offers dual-band functionality, its complexity and girth may still be limiting factors. Using a frequency-reconfigurable dual-band Plane Inverted-F Antenna (PIFA), [15] introduces a compact mobile device antenna system for LTE-M (0.7–0.9 GHz) and LTE2500 with a frequency-reconfigurable dual-band PIFA. The benefits include dual-band coverage for LTE-M and LTE-2500, which enables flexible communication. However, adding varactor diodes and a decoupling circuit increases its complexity and may reduce its overall efficiency. An elliptical patch and a split-ring resonator (SRR) [16] make a nonuniform meandered line shunt capacitive RF-MEMS switch. This design attains two states with distinct resonant frequencies, allowing for frequency reconfiguration. Due to the use of Al3N4 as the dielectric substance, the benefits include enhanced isolation. The disadvantage is the high voltage requirement for toggling between the ON and OFF states (7.9 volts). It is notable that most published works on reconfigurable-antennas utilize singular patch antennas, which may be large and have limited bandwidth. Researchers may investigate new techniques and designs for reconfigurable applications to improve the efficiency of single-patch antennas.

Wireless technologies that rely on a wide bandwidth for effective data transmission can use reconfigurable MIMO antenna systems because they have the inherent flexibility to modify and adapt their operational frequencies. Numerous frequency reconfigurable MIMO antenna designs have been published and are extensively documented in [17–22]. [17] proposes a reconfigurable full-metal-rimmed MIMO antenna for WWAN/LTE portable devices. Two center-symmetrically distributed antennas and radiation structure use the unbroken metal rims in a plastic case. The U-shaped feeding line couples the antenna element and generates a four-loop resonant mode. These hepta band MIMO antennas can cover GSM 850/900 and GSM 1800/UMTS/LTE 2500 by combining these four resonant modes using the reconfigurable method. [18] describes a low-profile 2×2 MIMO antenna design for metallic smartphone platforms that works across the entire long-term evolution (LTE) spectrum from 699–960 MHz to 1710–

2690 MHz. The method uses the longitudinal edges of the ground plane with a 2 mm ground clearance. The smartphone's metal frame and stub network create a reconfigurable linked-loop antenna structure. Reference [19] reconfigures a two-element MIMO antenna at 600 MHz, 1.8 GHz, 2.4 GHz, 3.5 GHz, and 5.5 GHz. The antenna layout includes two semicircular ring-shaped strip lines, a rectangular slit on the upper conducting layer of the substrate, and a U-shaped slot on the bottom. A single-pole, four-throw RF MEMS switch changes frequency. This reconfigurable antenna design may have performance, efficiency, and practicality issues that need further exploration.

A planar inverted-F antenna (PIFA) mobile handheld device based on dual ports and frequency tunable is described in [20]. MIMO antennas improve signal diversity and spatial multiplexing using two symmetrical PIFAs at 43.0 mm center-to-center distance. By changing v1 and v2 capacitance from 4.15 pF (0 V) to 0.72 pF (15 V), dual-band tunability is possible. Like any complex technical design, this dual-frequency tunable antenna system may have inherent flaws, requiring careful analysis of its operational performance, stability, and potential trade-offs. [21] proposes compact and high-isolation 2×2 MIMO antennas for industrial, scientific, and medical (ISM) band and 5G lower frequency band applications. These applications struggle with mutual coupling. Electromagnetic bandgap (EBG) based on a mushroom and a fractal-shaped structure have been studied to isolate the MIMO antenna elements with the isolation of -24.67 dB. [22] presents a 2.45/5.5 GHz WLAN CPW-fed dual-band antenna. Two identical trapezoidal elements are perpendicular in the MIMO antenna. The antenna's impedance bandwidth covers IEEE 802.11 a/b/g frequency bands of 2.25–3.15 GHz and 4.89–5.95 GHz. A rectangular microstrip stub provides less than -15 dB isolation in both operation frequency ranges.

Most previous research has addressed MIMO antenna system limitations like non-continuous frequency tuning, narrower bandwidth, no ground plane slits, large form factors, and inadequate radiating element isolation. This paper addresses these issues and proposes a small, continuously tunable, wide bandwidth antenna with high isolation between elements. A modified inverted F-antenna structure with a slit defective ground structure (DGS) and orthogonal alignments overcome these difficulties in the proposed design. One antenna is placed along the system plane's long edge, and the other on the substrate's top or lower surface. Each antenna element has a varactor diode as a reactive load to tune the frequency. The varactor diode can be biased to tune the antennas from 4.3 to 6.5 GHz.

The key novelties of our design are compact form factor, dual-polarizations, integrated MIMO design, practical implementation, mutual coupling consideration, and application perspective. Its planar-shape, compact size, and wide tuning across multiple frequency bands make it ideal for wireless communication front-end solutions. Thus, our MIMO antenna system advances wireless communication technology's performance and efficiency.

2. THE GEOMETRY OF THE DUAL POLARIZED SYSTEM

The top and side views of the dual-port reconfigurable antennas with fabricated prototype along with the feeding network for the varactor diode are shown in Fig. 1. The proposed system consists of dual modified inverted-F antennas placed on a $15 \times 25\,\text{mm}^2$ ground plane and implemented on a 0.8 mm thick Rogers RT5880-substrate with relative permittivity of 2.2 and tangent loss of 0.0009. The designed structure is a combination of two antennas. One antenna is situated on the exterior surface of the side-edge frame, while the other is positioned on the substrate surface. Each antenna has a rectangular shape shorted to the ground and an L-shaped parasitic radiator. Both sides of the substrate have been designed with clearance areas for 2G, 3G, and 4G wireless networks.

The antenna design process is depicted in Fig. 2, offering a comprehensive portrayal of the successive steps involved. In the initial stage (step 1), a 50-ohm microstrip line is the source for supplying the antenna, which is further equipped with a stub designed for impedance matching (step 2). However, a complication arises due to the imbalanced impedance exhibited by the surface beneath the radiating patch antenna, leading to an unresponsive radiator across the entire frequency spectrum.

To address this challenge, a rectangle-shaped patch is introduced and affixed to the ground plane below the edge of the radiator, thereby achieving an impedance match between the feed-line and the patch. This consequential improvement can be observed in Fig. 2(c), shedding light on step 3 of the process.

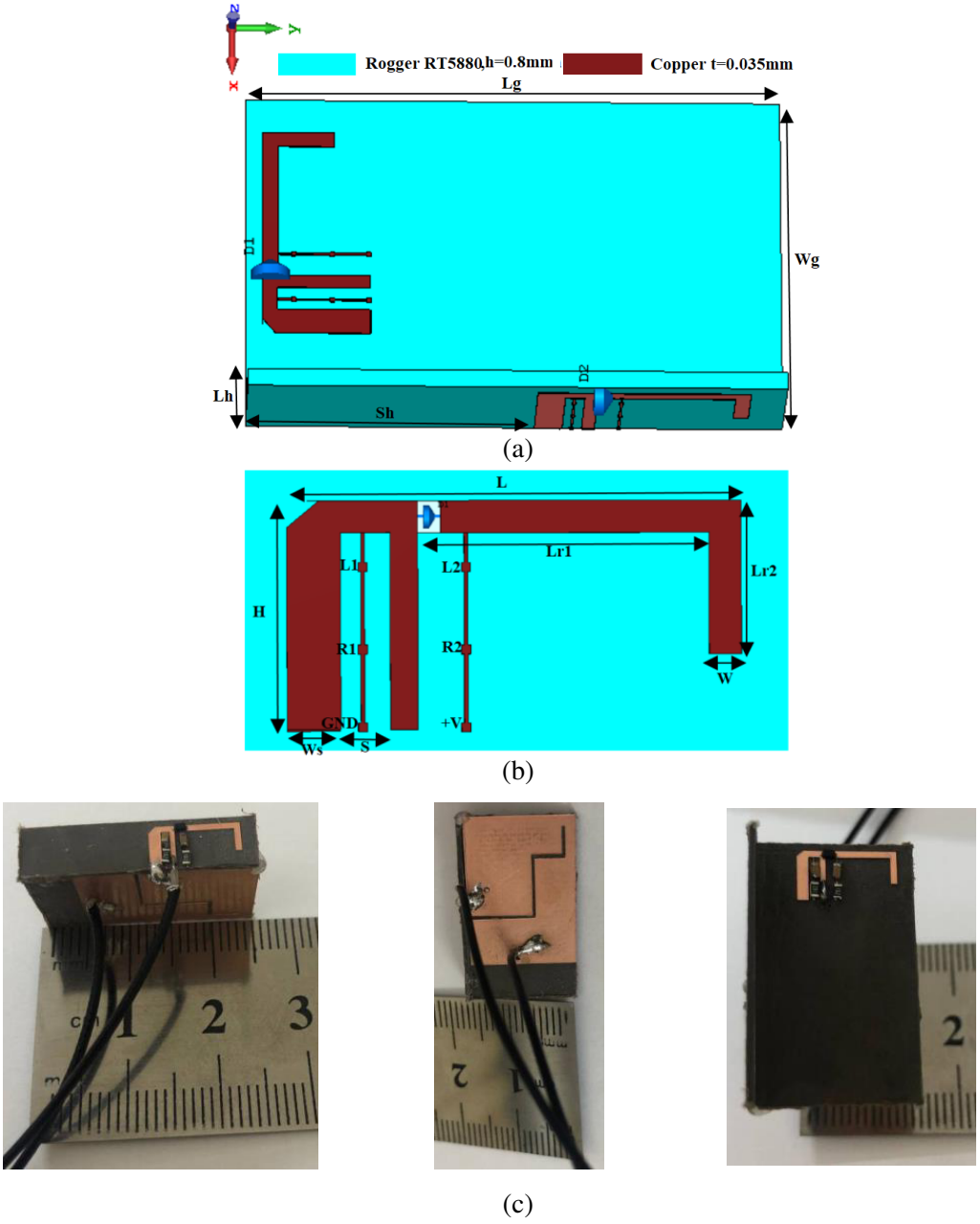

Figure 1. Geometry of dual-polarized MIMO antenna design: (a) Two-element, (b) single-element and (c) fabricated prototype.

Continuing with the sequence, Fig. 2(d) reveals the subsequent step (step 4), wherein an L-shaped parasitic element is interconnected with the primary radiator through a stub, facilitating its operation in the higher frequency band. This configuration is visually elucidated in the accompanying Fig. 3, which clearly explains this aspect.

In order to ensure the optimal functioning of the stub, a miter set at an angle of 45° is implemented, serving as a safeguard against micro-bending at the right angle. This precautionary measure effectively restricts the current flow on the stub, consequently attaining a desirable outcome (step 5).

The miter's role is closely related to antenna structure and transmission by controlling electromagnetic wave propagation inside the antenna as a reflecting medium. Miters improve antenna isolation, mutual coupling, and radiation pattern aspects.

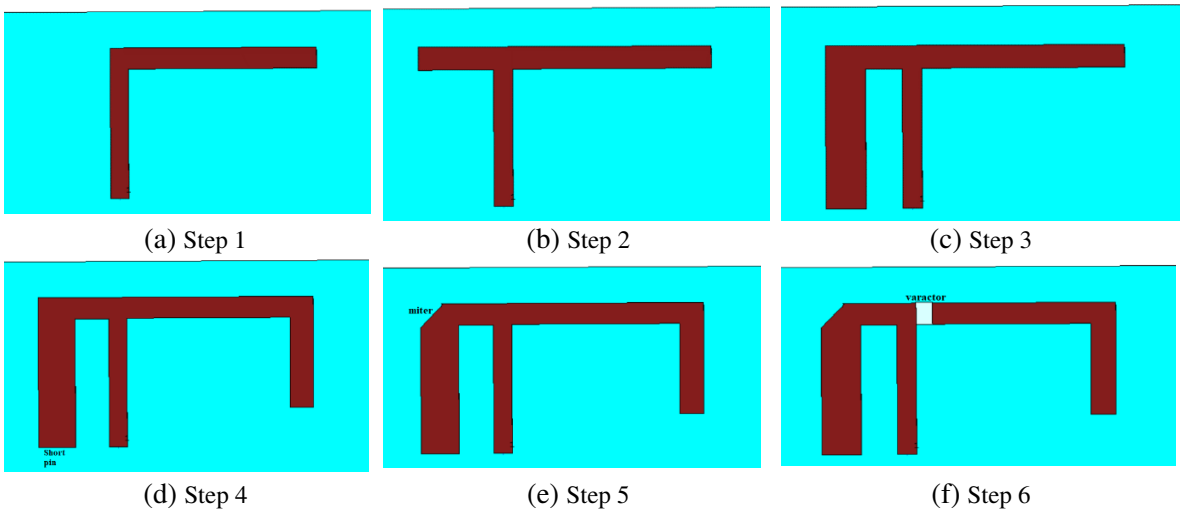

Figure 2. Antenna design process (six steps).

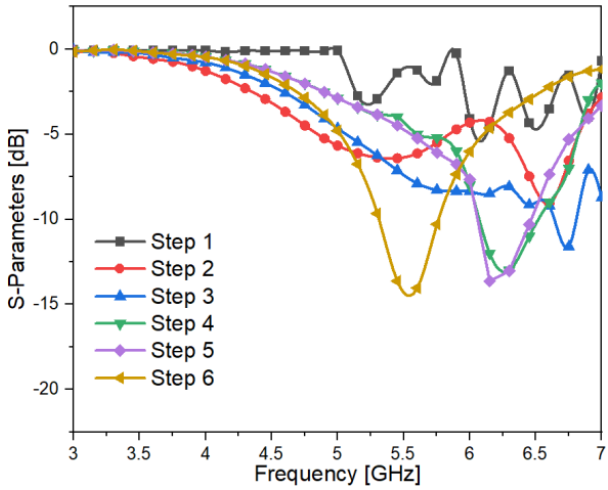

Figure 3. Reflection coefficients for the design process.

Various angles affect antenna reflection and scattering of electromagnetic waves. Simulations and optimization determined the 45° angle for optimal isolation, coupling, radiation pattern, and other factors. Variation from this angle may provide unwanted reflections or interference patterns, reducing antenna performance. The single miter location is a key to antenna performance. This placement reduces mutual interaction between antenna elements and directs radiation.

Moving forward, a precise gap measuring 0.8 mm is etched, accommodating varactor diodes between the main and parasitic L-shaped elements. This particular arrangement, presented in step 6 and accompanied by a capacitance of 0.7 pF, enables the antenna to operate seamlessly at a frequency of 5.5 GHz, an aspect vividly depicted in Fig. 3. The physical design of the antenna, the desired operational frequency range, and the necessary impedance characteristics to achieve maximum efficiency all play a role in determining where to place the varactor diode. The precise positioning of the varactor diode along the antenna's radiating element or feed structure enables the antenna's resonance frequency and impedance to be precisely adjusted. Consequently, this adjustment directly impacts the antenna's bandwidth and efficiency.

The design objectives and requirements determine where to place the single varactor diode on an

antenna. Although it is feasible to alter the antenna's position, such modifications should be performed with an in-depth knowledge of their impact on its overall performance.

Several important geometric parameters determine the resonant frequency of the modified inverted-Fractal Antenna (Fig. 1(b)). These parameters include patch length ($Lr1 + Lr2 = 8.2\,\text{mm} = L$), patch width ($W = 0.7\,\text{mm}$), shorting pin width ($Ws = 0.9\,\text{mm}$), dielectric layer height ($h = 0.8\,\text{mm}$), and pin height ($H = 4.1\,\text{mm}$).

The fundamental idea involves configuring the half wavelength of the shorting-pin from the opposite board edge. Observation reveals that the feed-point is positioned on the same side, and the feed is located at a distance of $S = 0.9\,\text{mm}$ from the short pin. It is notable that the Inverted-Fractal Antenna (IFA) is positioned at the height of H above the ground plane and on top of a dielectric material with a relative permittivity of 2.2.

By manipulating the feed distance to the short pin (S), it is possible to control the impedance characteristics of the IFA. In particular, bringing the input point closer to the shortening point will reduce impedance. The impedance can be enhanced by displacing it from the short edge, thereby enabling the parameter's tuning.

The design equation is [23]

$$Lr1 + Lr2 + W - Ws - S = \frac{\lambda}{2} + h + H \tag{1}$$

The first equation simplifies the two special cases that follow:

$$Lr1 + Lr2 = L = \frac{\lambda}{2} + h + H + S \qquad \text{for } W = Ws \tag{2}$$

$$Lr1 + Lr2 = L \approx -W + \frac{\lambda}{2} + h + H + S \qquad \text{for } Ws \approx 0 \tag{3}$$

The resonant frequency can be written as

$$f = \frac{C}{2\,(Lr1 + Lr2 + W - Ws - h - H - S)\,\sqrt{\varepsilon_r}} \tag{4}$$

where ε_r is the relative permittivity of the substrate, and c is the speed light.

2.1. Ground Plane Structure

An important feature of the modified antenna is its ground plane, which facilitates the input excitations of ground current. The ground plane exhibits ideal reflective behaviour when it has an infinite size or is

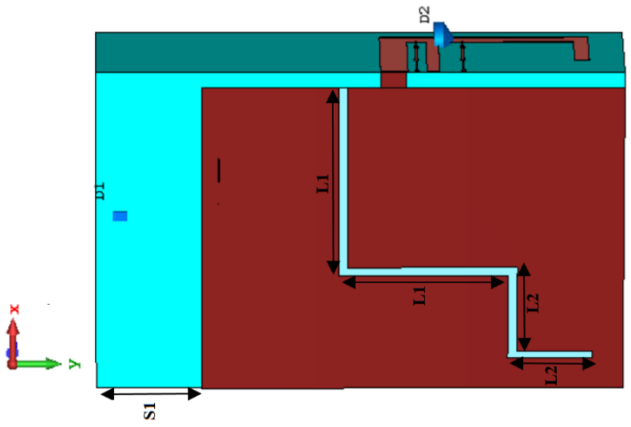

Figure 4. The defected ground of the design.

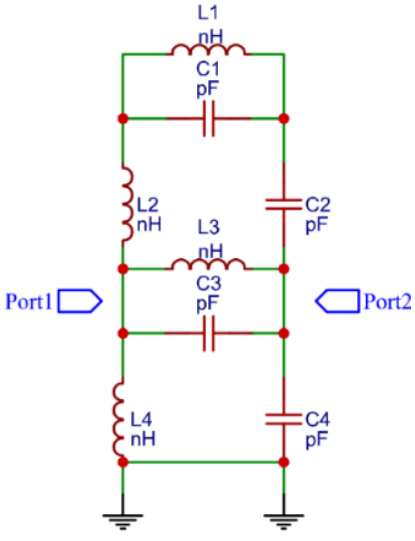

Figure 5. Equivalent circuit of isolation.

substantially larger than the radiator. Typically, the requisite length of the ground plane is about half of the wavelength. If the length exceeds $\lambda/2$, the inverted-FA radiation pattern will exhibit additional side lobes. Conversely, if the length is significantly shorter than $\lambda/2$, antenna calibration becomes difficult, resulting in a decline in overall output [24]. As shown in Fig. 4, the DGS, approximately $\lambda/2$ in length, has been removed from beneath the antenna to ensure the proposed system's desirable performance regarding isolation between antenna bandwidth and radiation pattern. Fig. 5 depicts the equivalent circuits of the DGS between elements. The values of S-parameters, which quantify the interaction between the incident and reflected waves at the antenna ports and their components, were obtained using the CST tool. Subsequently, these values were assigned using the ADS tool. The values, as mentioned, play a crucial role in the analysis of the antenna's behavior across various configurations, as well as in the evaluation of its performance within a circuit.

2.2. Equivalent Circuits of the Proposed Design

To accomplish efficient radiation, the antenna must possess favorable radiating characteristics, such as the synchronization of currents (electrical fields) and the capacity to efficiently transfer power from the transmission line to the antenna [24]. This necessitates minimizing the reactive component of the impedance, which can be accomplished through the equivalent circuit. Fig. 1(b) depicts a shorted strip line that adds parallel inductance to the antenna impedance at a fraction of a wavelength. Similarly, the antenna trace's open circuit generates capacitance to the left of the input point. The location of the feed is determined to balance capacitance and inductance on each side. Therefore, capacitance and inductance cancel each other out, leaving only radiation resistance.

To fine-tune the performance of the MIMO system, the equivalent circuit model depicted in Fig. 6 is employed and modified with the aid of an advanced design simulation (ADS) tool. CST and ADS are two prevalent design platforms for microwave components. Therefore, the values designated for each component must be derived from CST and then implemented in ADS. Reoptimization of these circuit components is required for accurate results in ADS.

Figure 7 compares the responses of the circuit and CST simulation. Notably, the circuit response in ADS exhibits a frequency shift toward the lower end along with a higher isolation parameter than the response simulated by CST. An impedance of 50 ohms represents each terminal. Obtaining precise equivalent values from CST is essential for achieving accurate results in ADS. Changes in inductance directly influence an antenna's resonance frequency and impedance matching, consequently affecting

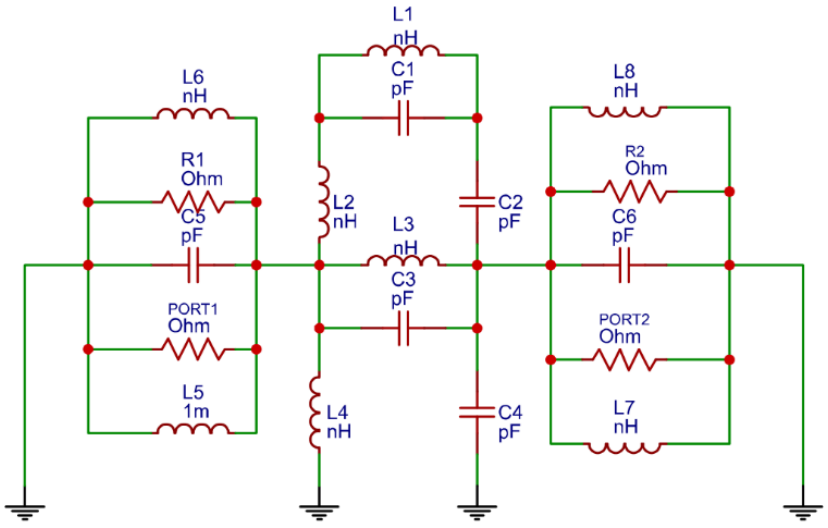

Figure 6. Equivalent circuit of dual-antennas with values: $L1 = L3 = 0.95\,\text{mH}$, $R1 = R2 = 50\,\text{Ohm}$, $C1 = C3 = 2.76\,\text{pF}$, $C2 = C4 = 2.1\,\text{pF}$, $L2 = L4 = 0.42\,\text{mH}$, $C5 = C6 = 3.0\,\text{pF}$, $L5 = L7 = 1.42\,\text{nH}$, $L6 = L8 = 1.4\,\text{nH}$.

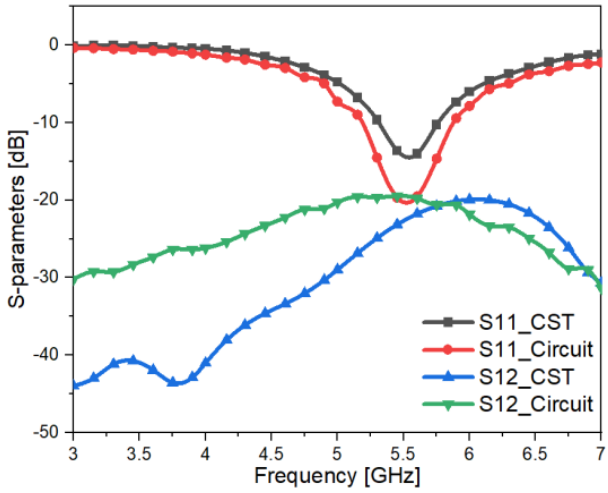

Figure 7. The response of circuit using ADS and CST.

its bandwidth with a minor change. Altering capacitance has a significant effect on the bandwidth and frequency values. Achieving optimal performance over the appropriate frequency range requires a balanced combination of inductance and capacitance.

3. RESULTS OF THE DUAL-POLARIZED SYSTEM

3.1. *S*-Parameters

A reconfigurable dual-port antenna design was simulated and optimized using a full wave electromagnetic simulator, specifically CST. As shown in Fig. 8, the CST tool analyzed the reflection coefficient. Following the datasheet, the frequency tuning was investigated by altering the capacitance values of the varactor diode within the range of 0.4 to 1.8 pF.

To validate the simulation results obtained from CST, we fabricated a prototype of the system, as shown in Fig. 1(c) and conducted measurements using the vector networks analyzer (VNA) model KC901V, covering the frequency range of 100 MHz to 7 GHz. The VNA was calibrated using a short open load through a calibration procedure prior to measurement. Modulating the reverse bias voltage applied

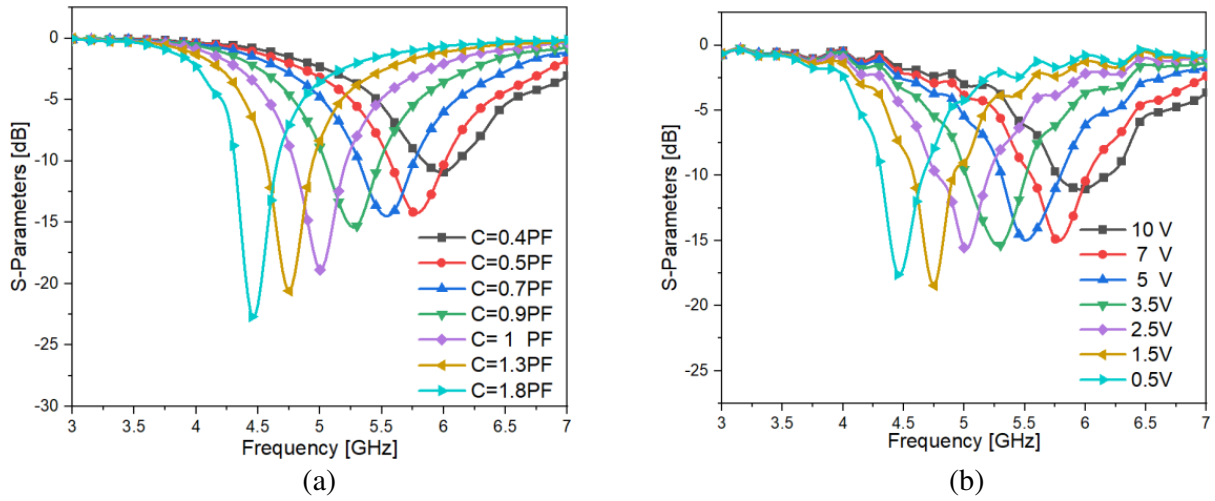

Figure 8. Simulated and measured reflection coefficients: (a) simulated and (b) measured.

to the varactor diode from 0.5 to 10 V yielded the measured reflection and transmission coefficients. The lower limit of the bias voltage is 0 V, according to the datasheet of the varactor diode SMV2019. This value decreases the resonance frequency by 0.25 GHz.

Figure 8 depicts a comparison between the antenna's simulated and measured reflection coefficients. By adjusting the reverse biased voltage of the varactor diode within the specified range (0.5 to 10 V), it is found that the lower and upper resonant bands could be tuned from 4.3 to 4.7 GHz and 5.55 to 6.5 GHz, respectively.

This section explicitly discussed three voltage cases (2.5, 3.5, and 10 V) for clarity and comprehension. At a capacitance value of 0.4 pF, the simulated antenna operated between 5.55 and 6.5 GHz, exhibiting a 10-dB bandwidth of 450 MHz for the upper resonant band, which corresponds to a fractional bandwidth of 7.8%. Similarly, the simulated antenna operated between 5 and 5.5 GHz with a 10-dB bandwidth of 500 MHz for the lower resonant band, representing a fractional bandwidth of 9.5% at a capacitance value of 0.9 pF. At 1.8 pF, the simulated antenna operated between 4.3 and 4.7 GHz, with a 10-dB bandwidth of 390 MHz for the lower resonant band, corresponding to an 8.8% fractional bandwidth.

In addition, the measured and simulated transmission coefficients (S_{12}) for the same three voltage instances are shown in Fig. 9. Notably, the measured transmission and reflection coefficients closely matched the predicted values. Minor variations in resonant frequency and bandwidth are caused by manufacturing tolerance, the effects of lumped elements in the biasing network, SMA and cable defects, and the soldering of diodes.

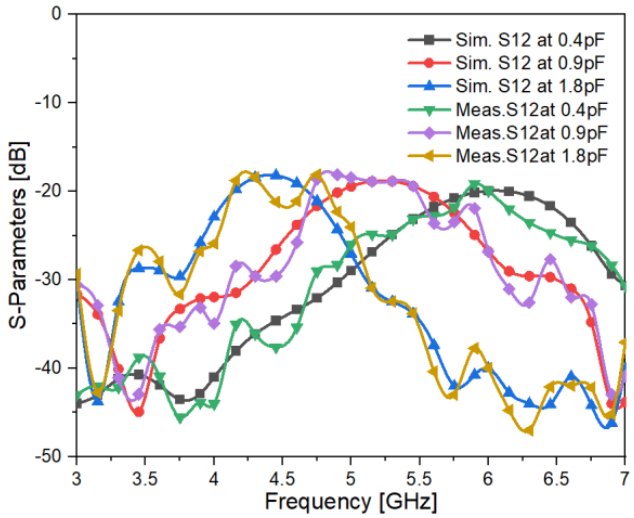

Figure 9. Measured transmission coefficients.

3.2. Diversity Performance of the Proposed Design

The envelope correlation coefficient (ECC) and diversity gain (DG) can be used to evaluate the diversity performance of a MIMO antenna. It is possible to determine the degree of spatial correlation or diversity between two antenna elements by performing an ECC calculation. For low-efficiency MIMO antennas, S-parameters cannot be used to calculate ECC [23]. So, for low efficiency antennas, the ECC should be estimated from the radiation patterns in the far field. ECC may be evaluated for high-efficiency antennas by determining the correlation of losses. A MIMO antenna with a radiation efficiency greater than 50% is well suited to this approach. The following equation can be used to obtain the guaranteed correlation coefficient [23]:

$$|\rho_{ij}|_{\text{guaranteed}} = |\rho_{ij}| + \sqrt{\left(\frac{1}{\eta_i} - 1\right)\left(\frac{1}{\eta_j} - 1\right)} \tag{5}$$

where

$$\rho_{ij} = \frac{-s_{ii}s_{ij}^* - s_{ji}s_{jj}^*}{\sqrt{\left(1-|s_{ii}|^2-|s_{ji}|^2\right)\left(1-|s_{jj}|^2-|s_{ij}|^2\right)\eta_i\eta_j}} \tag{6}$$

where η_i and η_i refer to the 1st and 2nd antennas, respectively. After figuring out the correlation coefficient, we can solve the following equation to find the guaranteed value of ECC:

$$\mathrm{ECC}_{\mathrm{guaranteed}} = |\rho_{ij}|^2 \text{ guaranteed} \tag{7}$$

This method of determining ECC between the two antenna elements is used since the designed MIMO antennas demonstrates greater than 84% efficiency in the operational bands. A total of ECC between antennas has been calculated and illustrated in Fig. 10. MIMO antennas with ECC values below 0.16 in both working bands meet the commonly accepted standard (ECC < 0.5) for the MIMO antennas performance [24].

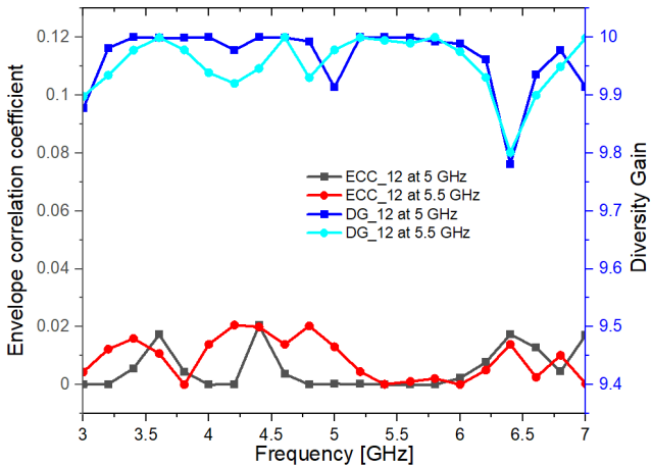

Figure 10. ECC and DG at 5 and 5.5 GHz.

As for evaluating the MIMO performance, the DG is another essential factor to consider. The DG shows how the elements outperform a single element in terms of performance. Ideal dynamic range of DG is 10 decibels. The computed DG is 9.96 dB, as shown in Fig. 10 using Equation (8) given below [24].

$$\mathrm{DG} = 10\sqrt{\left(1-|0.99\rho_{ij}|^2\right)} \tag{8}$$

3.3. Radiation Patterns and Efficiency

Figure 11 depicts the simulation and measurement of the E-theta and E-phi radiation patterns (co-polarization and cross-polarization) of the MIMO antenna at 5, 5.5, and 6 GHz. The horizontal and vertical antennas exhibit mutually complementary and symmetrical pattern, ensuring a high degree of pattern diversity and linear polarization purity.

The measured radiation pattern is obtained by enabling one antenna port while terminating the remaining ports with a 50 Ohm load. Throughout the investigations, a 1-meter separation was maintained between the transmitter and MIMO antennas under consideration. The designed MIMO system was rotated in both the E- and H-planes while the transmitter antenna remained stationary to collect signal intensity data.

Significantly, the E-phi component, which is aligned with the direction of the main lobe, has a greater intensity than the E-theta cross-polarization component. This attribute contributes to the attainment of desirable polarization and pattern diversity for the designed MIMO system, thereby enhancing its practical applications.

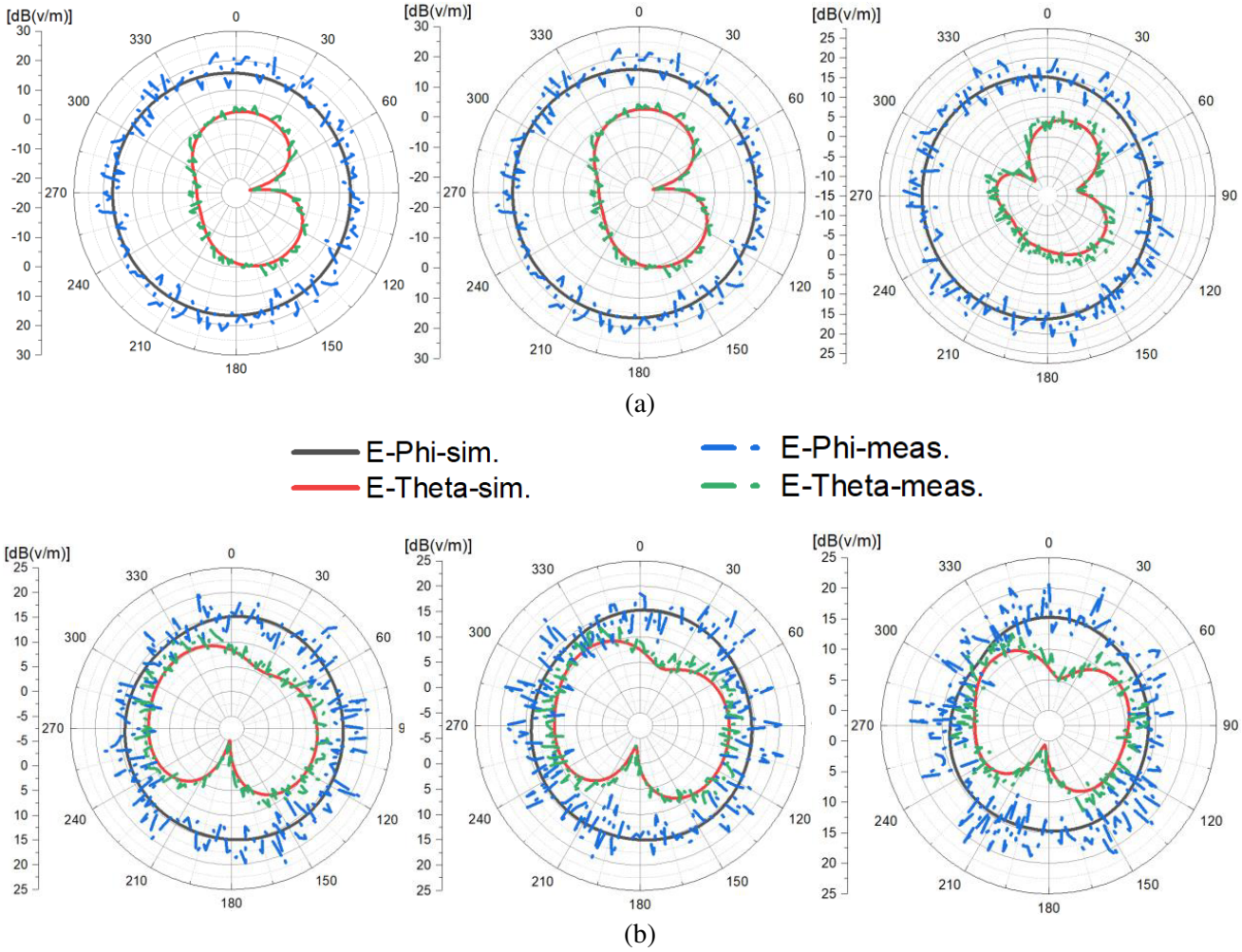

Figure 11. The simulated and measured radiation pattern of E-theta and E-phi at 5, 5.5, and 6 GHz: (a) Ant. 1 and (b) Ant. 2.

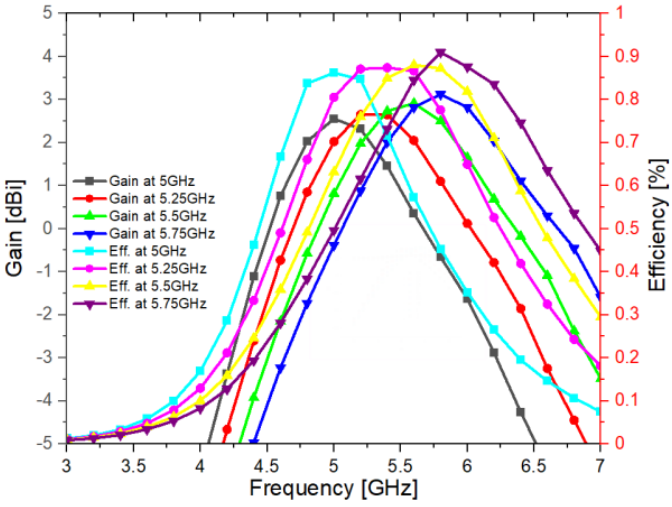

Figure 12. Gain and total efficiency for quad-states.

Figure 12 is a representation of the gain and total efficiency graphs for the four states of a varactor diode. For these states, the operating bands range from 4.78 to 5.21 GHz; 5 to 5.5 GHz; 5.3 to 5.75 GHz; and 5.55 to 6.5 GHz. Within these frequency ranges, the minimum gain and efficiency are 2.51 dBi and 84%, respectively. However, the highest gain is 3.2 dBi, and the maximum total efficiency is 90%. As shown, the total efficiency of the reconfigurable modified inverted-F antenna is improved when frequency increases.

4. COMPARISON WITH THE ANTENNAS REFERENCED

Table 1 compares the reconfigurable dual-polarized MIMO antenna to other antennas in the literature. The innovative antenna design has various advantages over existing ones. Dual radiators allow horizontal and vertical polarizations, improving link dependability.

Table 1. Performance comparison with previous works.

Ref.	No. of antennas	Element Size (mm^2)	PCB size (mm^2)	frequency (GHz)	Isolation (dB)	Gain (dBi)	Efficiency (%)	ECC	polarization
[17]	2	30×44	72×145	0.94, 1.86, and 2.63	> 11	1.4, 1.6, and 4	43, 59, and 72	< 0.33	1
[18]	2	50×9	70×150	0.69–0.96, 1.7–2.69	> 11	0.9–2.3, 2–3.6	70–80	< 0.5	1
[19]	2	32×50	32×98	0.6, 1.8, 2.4, 3.5, and 5.5	> 15	3–4	59–76	< 0.1	1
[20]	2	19×37	63×100	0.8, 0.98, 1.65, and 2.2	> 20	1.6–3.4	55–75	< 0.2	1
[21]	2	28×38	38×95	2.43–2.50	> 18	4–4.3	52–55	< 0.1	1
[22]	2	20×25	50×50	2.45 and 5.5	> 15	2–5	77–80	< 0.1	1
Prop. work	2	8.2×4.1	15×25	4.5, 5, 5.25, 5.5, 5.75, and 6	> 18	2.5–3.2	84–90	< 0.02	2

The optimized parameters and ground plane slit with dimensions almost equivalent to $\lambda/2$ have resulted in broad bandwidth covering six bands, high efficiency of more than 84%, and effective isolation of over 18 dB. This optimization was done without compromising the antenna's size, simplicity, or radiation performance.

Radiating elements arranged vertically and horizontally provide additional polarization vectors. This orthogonal antenna alignment creates pattern variety, which isolates radiators without complex decoupling parts.

Moreover, the proposed MIMO antenna system can be deployed on mobile terminals due to its compact area of $15 \times 25\,mm^2$.

5. CONCLUSION

This paper presents compact reconfigurable dual-port antennas with orthogonal arrangements for sub-6 GHz band applications. The antenna has successfully achieved tuning capabilities within the frequency range of 4.3 to 6.5 GHz by employing a single varactor diode and a simple biasing circuit. By integrating a dual-polarized configuration, the antenna provides improved diversity, which is essential for MIMO systems. The ability to independently control the polarization of the antenna's radiated signals offers greater flexibility and enhances the system's overall performance. Additionally, the 10-dB impedance has a transmission coefficient and ECC below -18 dB and 0.1, respectively, indicating good isolation and diversity. Its compact size with more than 82% total efficiency and gain of 3 dBi makes it suitable for sub-6 GHz mobile terminals.

ACKNOWLEDGMENT

The authors appreciate the help they received from Al-Iraqia University in Baghdad, Iraq (https://aliraqia.edu.iq).

REFERENCES

1. Kareem Al-Gertany, Q. H., M. J. Farhan, and A. K. Jassim, "Design and analysis a frequency reconfigurable octagonal ring-shaped quad-port dual-band antenna based on a varactor diode," *Progress In Electromagnetics Research C*, Vol. 116, 235–248, 2021.
2. Tawk, Y., M. Bkassiny, G. El-Howayek, S. K. Jayaweera, K. Avery, and C. G. Christodoulou, "Reconfigurable front-end antennas for cognitive radio applications," *IET Microwaves, Antennas and Propagation*, Vol. 5, No. 8, 985–992, 2011.
3. Valenta, V., R. Maršálek, G. Baudoin, M. Villegas, M. Suarez, and F. Robert, "Survey on spectrum utilization in Europe: Measurements, analyses and observations," *2010 Proceedings of the 5th International Conference on Cognitive Radio Oriented Wireless Networks and Communications, CROWNCom*, 2010.
4. Liu, L., S. W. Cheung, and T. I. Yuk, "Compact MIMO antenna for portable devices in UWB applications," *IEEE Transactions on Antennas and Propagation*, Vol. 61, No. 8, 4257–4264, 2013.
5. Zhang, S. and G. F. Pedersen, "Mutual coupling reduction for UWB MIMO antennas with a wideband neutralization line," *IEEE Antennas and Wireless Propagation Letters*, Vol. 15, 166–169, 2016.
6. Yang, H. H. and T. Q. S. Quek, *Massive MIMO Meets Small Cell?: Backhaul and Cooperation*, Springer Cham, 2017.
7. Li, H., J. Liu, Z. Wang, and Y.-Z. Yin, "Compact 1×2 and 2×2 MIMO antennas with enhanced isolation for ultrawideband application," *Progress In Electromagnetics Research C*, Vol. 71, 41–49, 2017.
8. Biswas, A. K. and U. Chakraborty, "Compact wearable MIMO antenna with improved port isolation for ultra-wideband applications," *IET Microwaves, Antennas and Propagation*, Vol. 13, No. 4, 498–504, 2019.
9. Majid, H. A., M. K. A. Rahim, M. R. Hamid, N. A. Murad, and M. F. Ismail, "Frequency-reconfigurable microstrip patch-slot antenna," *IEEE Antennas and Wireless Propagation Letters*, Vol. 12, 218–220, 2013.
10. Majid, H. A., M. K. Abd Rahim, M. R. Hamid, and M. F. Ismail, "Frequency reconfigurable microstrip patch-slot antenna with directional radiation pattern," *Progress In Electromagnetics Research*, Vol. 144, 319–328, 2014.
11. Yang, X., Y. Chen, L. Ye, M. Wang, M. Yu, and Q. H. Liu, "Frequency reconfigurable circular patch antenna using PIN diodes," *9th International Conference on Microwave and Millimeter Wave Technology, ICMMT 2016 — Proceedings*, Vol. 2, 606–608, 2016.
12. Mahlaoui, Z., E. Antonino-Daviu, A. Latif, M. Ferrando-Bataller, and C. R. Penafiel-Ojeda, "Frequency reconfigurable patch antenna using pin diodes with directive and fixed radiation pattern," *2018 International Conference on Selected Topics in Mobile and Wireless Networking, MoWNeT*, 2018.
13. Madhav, B. T. P., M. Monika, B. M. S. Kumar, and B. Prudhvinadh, "Dual band reconfigurable compact circular slot antenna for WiMAX and X-band applications," *Radioelectronics and Communications Systems*, Vol. 62, No. 9, 474–485, 2019.
14. Zhou, J., M. Yang, and J. Yu, "Pattern reconfigurable patch antenna with dual band characteristic for WLAN & 5G applications," *Progress In Electromagnetics Research M*, Vol. 98, 147–158, 2020.
15. Diallo, K., A. Diallo, I. Dioum, S. Ouya, and J. M. Ribero, "Design of a dual-band antenna system for lTE-M and LTE-MIMO by exploiting the characteristic mode theory," *Progress In Electromagnetics Research M*, Vol. 93, 11–21, 2020.

16. Sailaja, B. V. S. and K. K. Naik, "Design of elliptical-shaped reconfigurable patch antenna with shunt capacitive RF-MEMS switch for satellite applications," *International Journal of Microwave and Wireless Technology*, Vol. 13, No. 9, 969–978, 2021.
17. Xu, Z. Q., Y. T. Sun, Q. Q. Zhou, Y. L. Ban, Y. X. Li, and S. S. Ang, "Reconfigurable MIMO antenna for integrated-metal-rimmed smartphone applications," *IEEE Access*, Vol. 5, 21223–21228, 2017.
18. Choi, J., W. Hwang, C. You, B. Jung, and W. Hong, "Four-element reconfigurable coupled loop MIMO antenna featuring LTE full-band operation for metallic-rimmed smartphone," *IEEE Transactions on Antennas and Propagation*, Vol. 67, No. 1, 99–107, 2019.
19. Hassan, M. M., Z. Zahid, A. A. Khan, I. Rashid, A. Rauf, and F. A. Bhatti, "Two element MIMO antenna with frequency reconfigurable characteristics utilizing RF MEMS for 5G applications," *Journal of Electromagnetic Waves and Applications*, Vol. 34, No. 9, 1210–1224, 2020.
20. Shruthi, G. and C. Y. Kumar, "Dual-band frequency-reconfigurable MIMO PIFA for LTE applications in mobile hand-held devices," *IET Microwaves, Antennas and Propagation*, Vol. 14, No. 5, 419–427, 2020.
21. Sharma, K. and G. P. Pandey, "Two port compact MIMO antenna for ISM band applications," *Progress In Electromagnetics Research C*, Vol. 100, 173–185, 2020.
22. Dou, Y., Z. Chen, J. Bai, Q. Cai, and G. Liu, "Two-port CPW-fed dual-band MIMO antenna for IEEE 802.11 a/b/g applications," *International Journal of Antennas and Propagation*, Vol. 2021, 2021.
23. Kareem, Q. H. and M. J. Farhan, "Compact dual-polarized eight-element antenna with high isolation for 5G mobile terminal applications," *International Journal of Intelligent Engineering and Systems*, Vol. 14, No. 6, 187–197, 2021.
24. Balanis, C. A., *Antenna Theory: Analysis and Design*, John Wiley & Sons, 2016.